Local structure of $LiNiO_2$ studied by neutron diffraction

J.-H. Chung*
Department of Materials Science and Engineering and Laboratory for Research on the Structure of the Matter, University of Pennsylvania, Philadelphia, Pennsylvania 19104, USA

Th. Proffen
Lujan Center, Los Alamos National Laboratory, Los Alamos, New Mexico 87545, USA

S. Shamoto
Neutron Science Research Center, JAERI, Tokai, Ibaraki, 319-1195, Japan

A. M. Ghorayeb
Laboratoire Matériaux et Microélectronique de Provence, CNRS UMR 6137, Université d'Aix-Marseille III, Case 142, 13397 Marseille Cedex 20, France

L. Croguennec
Institut de Chimie de la Matière Condensée de Bordeaux, CNRS, 33608 Pessac Cedex, France

W. Tian
Department of Physics and Astronomy, University of Tennessee, Knoxville, Tennessee 37996, USA

B. C. Sales, R. Jin, and D. Mandrus
Oak Ridge National Laboratory, Oak Ridge, Tennessee 37831, USA
and Department of Physics and Astronomy, University of Tennessee, Knoxville, Tennessee 37996, USA

T. Egami
Department of Materials Science and Engineering and Department of Physics and Astronomy, University of Tennessee, Knoxville, Tennessee 37996, USA
and Oak Ridge National Laboratory, Oak Ridge, Tennessee 37831, USA
(Received 25 May 2004; revised manuscript received 8 November 2004; published 22 February 2005)

The nature of the magnetic state of $LiNiO_2$ has been controversial. In this compound Ni spins ($S=1/2$) form a triangular lattice with the possibility of magnetic frustration, but the exact state of spin correlation has not yet been known in spite of the extensive research work. A factor that complicates understanding of the magnetic state is the orbital state of Ni^{3+} which is a Jahn-Teller (JT) ion. While there is no signature of long-range Jahn-Teller distortion, local JT distortion has been suspected. We have performed neutron diffraction and atomic pair-density function analyses up to unprecedented large distances to discover a number of unusual features, such as anomalous peak broadening, local JT distortion, sharp oxygen-oxygen distance correlations, and inverted temperature dependence of medium range correlation. These observations are best explained by local orbital ordering of Ni^{3+} ions into three sublattices. This orbital ordering, however, cannot develop into long-range order because of the strain field it generates, and domains of about 10 nm in size are formed. Domains are susceptible to random pinning by impurities (site disorder) resulting in the loss of structural long-range order. We suggest that this local orbital ordering is the basis for the complex magnetic properties observed in this compound.

DOI: 10.1103/PhysRevB.71.064410 PACS number(s): 61.12.Ld, 71.27.+a, 71.70.Ej

I. INTRODUCTION

Frustrated magnetism is a subject of considerable research attention at present, not only because it is an interesting phenomenon, but also because frustrated spin systems are highly susceptible to perturbations and could lead to novel phenomena through interplay with other forces. A classic example of frustrated spin systems is antiferromagnetic Ising spins forming a triangle, where the third spin cannot be in a minimum energy configuration with both neighbors simultaneously. In the two-dimensional triangular lattice there are manifolds of possible ground states leading to the frustration of the whole system. In $LiNiO_2$ Ni^{3+} spins form two-dimensional triangular networks separated by Li layers, which provide a ground for geometrical frustration. It has earlier been suggested[1] as a candidate system for the exotic resonant valence bond (RVB) state[2] to occur. While the likelihood of the RVB state in this compound appears to be in doubt, a number of competing proposals on possible magnetic ground states have been suggested, including two-dimensional (2D) Ising ferromagnet,[3] frustrated antiferromagnet,[4–7] spin glass,[8–11] quantum disor-

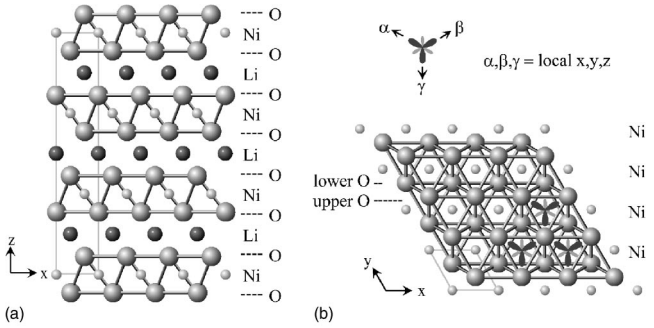

FIG. 1. (a) A side view of $LiNiO_2$ structure ($R\bar{3}m$) revealing stacks of NiO_2 slabs and Li layers. The thin solid lines connecting four Ni sites denote the boundary of a unit cell. (b) A top view of a NiO_2 slab showing the network of edge-shared octahedra. At the right bottom corner, the threefold arrangement of Ni $3d_{\alpha^2-r^2/3}$ ($\alpha = x$, y, or z) orbitals is also shown.

dered state,[12] etc., and the question is still wide open. Whereas these studies were restricted to low-temperature studies, a recent work[13] extended the measurement to high temperatures and proposed the possibility of orbital frustration, which would have significant impact on the magnetic properties. This proposal was based on the observation of anomalies in spin susceptibility at two distinct temperature scales, at 10 and at 400 K, which they interpreted as originating from spin interaction and orbital interaction, respectively. Ni^{3+} has d^7 configuration that splits into $t_{2g}{}^6$ and $e_g{}^1$ by the octahedral crystal field, so that it is a Jahn-Teller ion. They surmised that the local Jahn-Teller distortion[14,15] may be responsible for the large energy scale that produces the anomaly around 400 K. The primary purpose of the present work is to determine the orbital state of this compound through neutron diffraction, analyzed both in real and reciprocal spaces. The knowledge obtained in this work should facilitate understanding of the magnetic interactions in this system.

$LiNiO_2$ has a layered structure made of stacks of NiO_2 layers with intercalating Li layers [Fig. 1(a)]. Figure 1(b) shows the top view of the NiO_2 layer or slab with triangular symmetry. The building block of the NiO_2 layer is a NiO_6 octahedron, as is commonly found in transition metal oxides. Unlike the cuprates and manganites that have a corner-shared network of octahedra, $LiNiO_2$ has an edge-shared network of NiO_6 octahedra. The corner-shared network of MO_6 octahedra has linear M-O-M bonds, which can easily be buckled. However, in the edge-shared network two M ions are connected by two oxygen ions, so the network is much more rigid, and this has a major implication as we discuss below. Since Ni^{3+} is a strong Jahn-Teller (JT) ion, a topologically equivalent compound $NaNiO_2$ shows collective collinear JT distortion with variation in the Ni—O distance as much as 6%.[16,17] Since such a collective distortion has not been observed for $LiNiO_2$, it has often been assumed that in $LiNiO_2$ the JT orbitals are randomly oriented.[14,18] Structurally, however, the random orientation of the JT orbital in the rigid triangular network is very unlikely. There is also a speculation that the JT orbitals in $LiNiO_2$ order collinearly as in $NaNiO_2$ but their collective orientations split into nanodomains due to impurities. The purpose of the present work is to determine the local structure of $LiNiO_2$ by neutron diffraction and to investigate the possible connection between the observed magnetic property and the underlying orbital state. We show that the orientations of JT orbitals in $LiNiO_2$ are neither random nor collinear, but instead they form an ordered pattern that is compatible with triangular symmetry. The orbital ordering, however, is prevented from developing into long-range order because of the strain field it generates, and domains of about 10 nm in size are formed. We suggest that this local orbital ordering is the basis for the complex magnetic properties observed in this compound.

II. EXPERIMENTAL METHODS

Two different powder samples of $LiNiO_2$ were used in this study. One (sample 1) was prepared following the procedure described by Rougier *et al.*,[14] while the other (sample 2) followed the procedure by Bianchi *et al.*[19] $LiNiO_2$ tends to have Li and O vacancies which make it an ionic conductor.[9] Special care was taken to limit these vacancies to below 0.1%. Neutron powder diffraction profiles were obtained by the NPDF diffractometer at Manuel Lujan Neutron Scattering Center of Los Alamos National Laboratory. NPDF was recently upgraded by adding expanded backscattering detector banks with large arrays of ^{3}He position sensitive detectors that increased the data collection rate by more than a factor of 5.[20] A powder sample was sealed in a vanadium can with He heat exchange gas and placed in a cryofurnace. The measurements were made at various temperatures between 10 and 585 K. At each temperature data were collected roughly for 4 h, which produced excellent statistics suitable for both reciprocal space Rietveld analysis and real space atomic pair-density function (PDF) analysis. Additional background measurements were also made in order to obtain the structure functions purely from samples for the real space PDF analysis.

The reciprocal space Rietveld refinement analysis was performed with the GSAS package.[21] Only the histograms from the 90°-detector banks were chosen for the refinement, since the peak profile from conventional tube detectors can be precisely fitted with well-known pseudo-Voigt functions. It was assumed that the major defect is Ni_{Li}, so the formula is $(Li_{1-x}Ni_x)NiO_2$. Under this assumption, the defect concentration of sample 1 was estimated to be $x=0.0235\pm0.004$ from the Rietveld refinement. The sample 2 had a higher defect concentration $x=0.0388$. We note that we also have tried other possibilities, such as $(Li_{1-x}Ni_x)(Ni_{1-x}Li_x)O_2$ or $(Li_{1-x}Ni_x)(Ni_{1-y}Li_y)O_2$. Naturally, the latter gave the best agreement factor, since it has higher number of refinable parameters. However, it is reasonable to assume that the major point defect in this sample is the Ni_{Li}, since Li^+ ion is too large to enter the Ni^{3+} site. In any case, the estimated defect concentration was well below 3% for the sample 1.

The atomic pair density function (PDF) which is the Fourier transformation of the neutron diffraction profile, was calculated by the following equation:

$$G(r) = 4\pi r\rho_0[g(r) - 1] = \int_0^\infty Q[S(Q) - 1]\sin(Qr)dQ, \tag{1}$$

where $g(r)$ is the pair distribution function, ρ_0 is the average atomic density, and $S(Q)$ is the normalized structure function determined from the diffraction intensity.[22] The diffraction data were processed using the PDFGETN program.[23] Since the signal to noise ratio deteriorates quickly with increasing Q, it is advantageous to introduce cutoff in Q, which was chosen to be 35–40 $Å^{-1}$ in this study. At the same time a theoretical pair distribution function can be calculated by the following formula, which serves as the basis for the refinement:

$$G_{\text{calc}}(r) = \frac{1}{rN}\sum_{i,j}\left[\frac{b_i b_j}{\langle b\rangle^2}\delta(r - r_{ij})\right] - 4\pi\rho_0, \tag{2}$$

where b_i and r_{ij} are the scattering length of ith atom and the distance between ith and jth atom, respectively, and N is the number of atoms. In real data, the distance correlations expressed as δ functions in Eq. (2) are broadened due to thermal fluctuations. This effect is described by convolution with Gaussians with certain widths determined by the Debye-Waller factors.

The PDF has traditionally been used for the analysis of local structure up to 10 Å or so. However, we note that in this work we determined and analyzed the PDFs up to very large distances as have never been done before. The accuracy of the PDF in terms of distances is related to the resolution in Q. Just as the real space uncertainty due to lattice vibration becomes the multiplicative Debye-Waller factor upon Fourier transform, ΔQ translates to an envelope function for the PDF.[22] In a time-of-flight spectrometer used for pulsed neutrons ΔQ is proportional to Q and deteriorates at high Q, limiting the range of the PDF in distance. The NPDF spectrometer has a very high resolution of $\Delta Q/Q = 0.0015$ at backscattering, allowing the PDF to be determined accurately up to very large distances.[20] This enables seamless structural characterization ranging continuously from the local structure to the medium-range and long-range structure. For the purpose of comparison, especially for the long-range PDF peaks, we also have measured the neutron diffraction of $LiVO_2$ and $Na_{0.75}CoO_2$. The former has exactly the same crystal structure and space group as far as average structure is concerned, while the latter has the space group $P6_3/mmc$ but a similar triangular symmetry with edge-shared octahedra. The measurements of these compounds were done at 12 and 290 K using a closed cycle refrigerator.

III. EXPERIMENTAL RESULTS

A. Rietveld refinement of neutron diffraction

For the analysis of the structural change with temperature, we began with refining the neutron-diffraction data with the Rietveld method at a temperature in the middle of the range studied, 335 K, and proceeded by applying the obtained diffraction peak profile parameters for the data at different temperatures. The space group of $LiNiO_2$ was initially assumed to be $R\bar{3}m$ as has been previously assumed.[18] At the temperature range above 335 K, the refinements with the fixed set of profile parameters produced reasonably good agreements, confirming that the structure was essentially $R\bar{3}m$. However, the agreement deteriorated as the temperature was lowered. Further refining of sample-dependent profile parameters at each temperature could bring only partial improvement. Figures 2(a) and 2(b) show the neutron-powder-diffraction patterns and their refinements with the $R\bar{3}m$ symmetry at 335 and 10 K, respectively. As is easily noticed agreement is quite poor for 10 K. The major source of disagreement is anomalous peak broadening for some peaks.

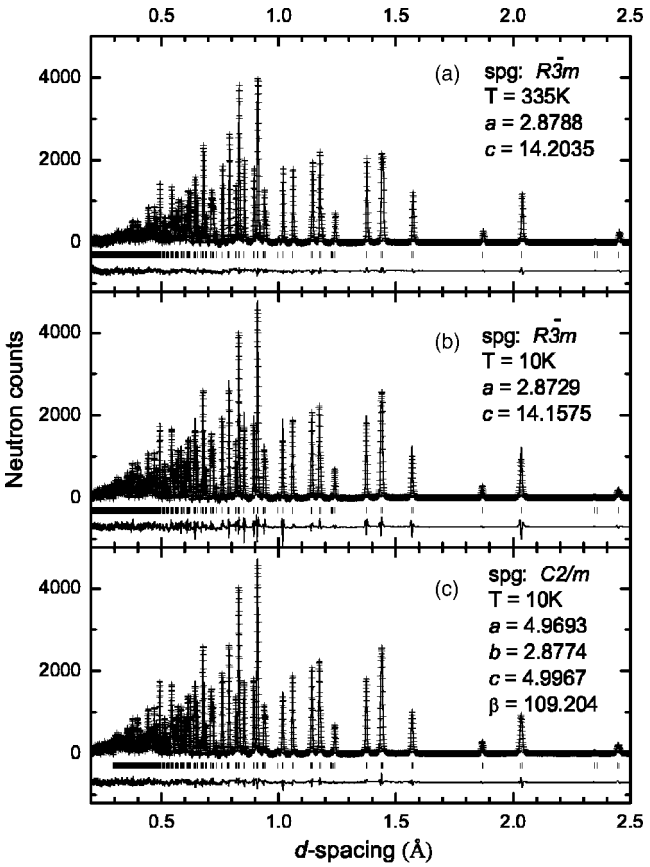

FIG. 2. The Rietveld refinement analysis of the neutron-diffraction profile from $LiNiO_2$ (sample 1). Refinement was done with the space group for (a) and (b), while the space group $C2/m$ was used for (c).

Figure 3(a) shows the temperature-dependent peak broadening of the (1 0 4) reflection, which showed the largest change with temperature. The anomalous shape of the (1 0 4) peak has been reported for room temperature x-ray-diffraction measurement on $Li_{0.93}Ni_{1.07}O_2$, from which the authors suggested the existence of two phases as an origin of the peak broadening.[24] However, in the present study with low defect concentrations, we can safely rule out this possibility since we did not observe extra reflections or linearly Q-dependent broadening which would implicate the presence of a second phase. The systematic peak broadening, as summarized in Figs. 3(b) and 3(c), was quite different from what we would expect from the two-phase behavior. In this plot,

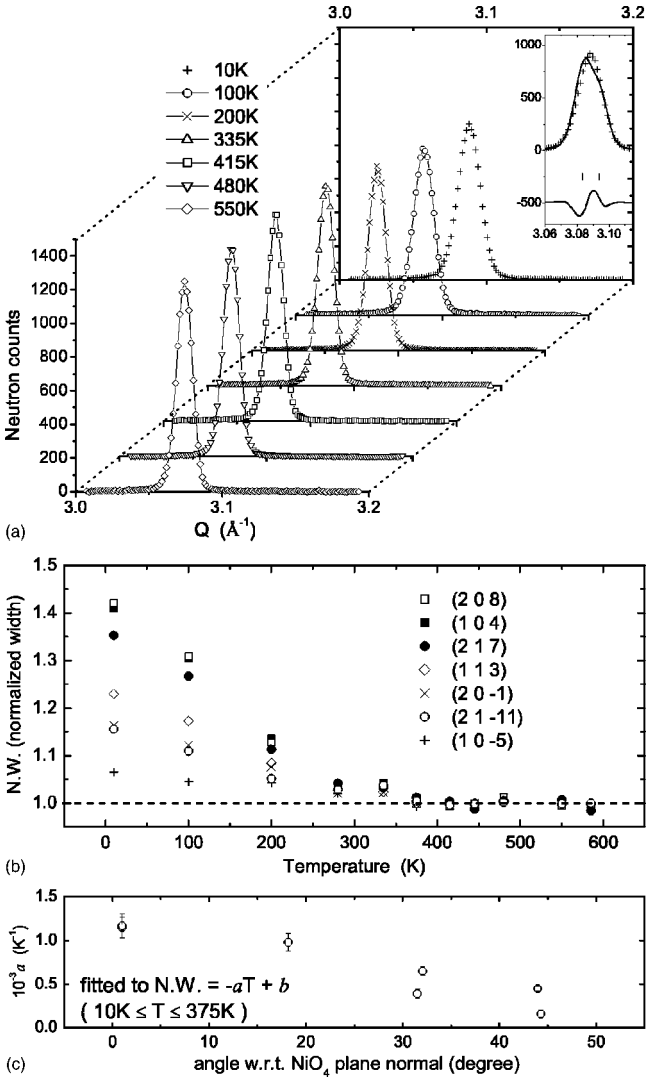

FIG. 3. (a) Temperature-dependent peak broadening observed for the (1 0 4) reflection of the neutron-diffraction profile of $LiNiO_2$. The inset is the comparison between the measured profile at 10 K and the calculated one based on $C2/m$ space group. (b) The normalized peak widths of the reflections in the neutron diffraction profiles of $LiNiO_2$ obtained by Gaussian fitting. The obtained peak widths at each temperature were normalized to the average of those beyond 400 K. (c) The slope of the temperature-dependent peak widths as a function of the angle between the momentum vector and Ni—O bond direction.

the width of each reflection was normalized to an average between 400 and 585 K, where the peak broadening is negligible. While the peak widths apparently are not systematically dependent on the magnitude of the reciprocal vector **Q**, they were found to be strongly dependent on its direction. Figure 3(c) shows the slopes of the peak widths, obtained by fitting to Fig. 3(b) between 10 and 350 K and plotted as functions of the angle that **Q** makes with the [1 0 3.86] reciprocal vector, which is along the three equivalent O—Ni—O bonds within the NiO_6 octahedra. The plot shows that the broadening is more pronounced for the reflections closer to the orientation of the O—Ni—O bonds, strongly suggesting relations to the medium-range ordering

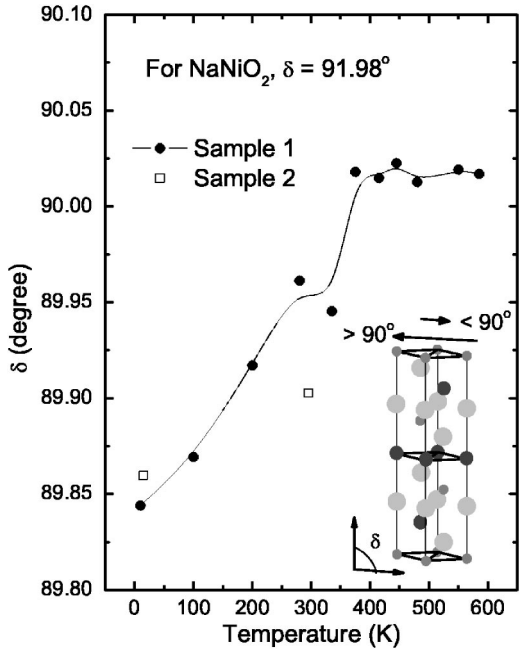

FIG. 4. Temperature dependence of angle δ deduced from Rietveld refinement with $C2/m$ model. The meaning of the angle δ is shown in the inset. Closed circles and open squares are from samples 1 and 2, respectively. The sold line is a guide to the eye through sample 1. The large arrow above the unit cell is the Jahn-Teller-induced shear observed in $NaNiO_2$, while the small arrow is the strain-induced monoclinic shear observed in $LiNiO_2$.

of local Jahn-Teller orbitals. It is certainly inconsistent with random orientation of local JT distortions, which will result in anisotropic thermal factors but not in peak broadening.

Based on this idea, we tried the Rietveld refinement with the $NaNiO_2$-type $C2/m$ monoclinic model and the result is shown in Fig. 2(c). Interestingly, the broadening of the peaks was well accommodated into the $C2/m$ structure, and a substantially better agreement was achieved. While such monoclinic distortion is observed for $NaNiO_2$ which shows collective Jahn-Teller distortion,[16] this does not imply the homogeneous $NaNiO_2$-type distortion as the ground-state structure of $LiNiO_2$. First, the magnitude of the monoclinic shear in $LiNiO_2$ is smaller than that in $NaNiO_2$ by more than an order of magnitude. More importantly, the sense of the monoclinic shear is opposite to that in $NaNiO_2$. As a result, the structure shows almost no, or inverse, Jahn-Teller distortions with two Ni—O bonds at 1.96 Å and four at 1.97 Å. Figure 4 shows the angle δ as a measure of monoclinic shear deduced from the $C2/m$-based Rietveld refinement with the peak profile parameters fixed. It is apparent that below 380 K the shear has a small negative linear dependence on the temperature, but the direction is opposite from what is expected for the collinear Jahn-Teller distortion. The amount of distortion deduced from the Rietveld refinement is as small as −0.16° at 10 K, compared to +1.98° for $NaNiO_2$.[16] Therefore, it is apparent that the actual local orbital ordering in $LiNiO_2$ is dramatically different from the case of $NaNiO_2$. We note that the obtained δ as plotted in Fig. 4 may even be an overestimate, and true values may be smaller in magnitude by as much as 30%, because we could obtain smaller

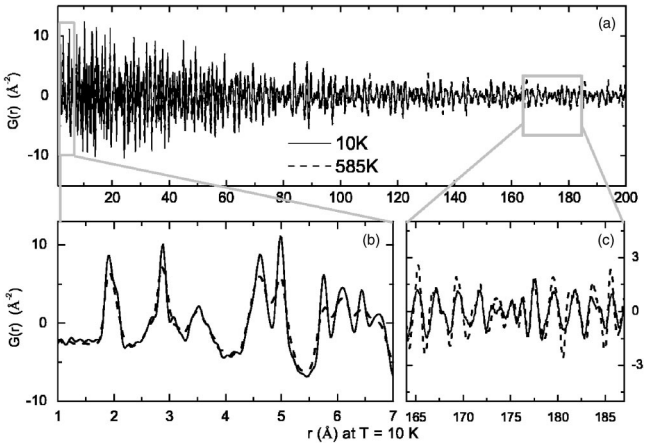

FIG. 5. The neutron pair density functions of $LiNiO_2$ (sample 1) measured at 10 and 585 K. The *x* axis for the 585 K data is scaled considering the lattice constant expansion. The PDF peaks are clearly seen up to as high as 200 Å.

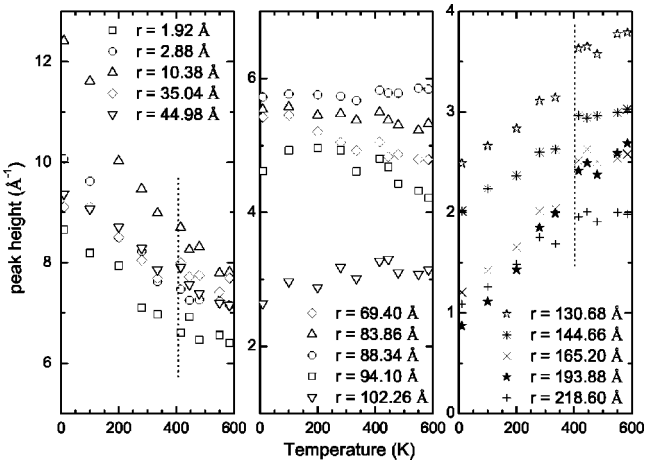

FIG. 6. The temperature-dependent peak heights obtained from the pair density functions $G(r)$ of $LiNiO_2$ at (a) short range, (b) medium range, and (c) long range. The dotted vertical lines are drawn to highlight the saturation behavior above $T=400$ K.

distortions along with better agreement factors by fully refining peak profile parameters under the monoclinic model. In this case, however, we often found multiple local minima with similar *R* factors but with large variance in the obtained crystallographic parameters. This ambiguity must be the result of having a large number of refinable parameters, and we will not present the result here. The details of the peak shape also argue against the presence of a monoclinic unit cell. The inset in Fig. 3(a) shows the measured (1 0 4) reflection at 10 K superposed on the refinement with the monoclinic model. While the monoclinic model expects unequal weights for the split peaks, the measured profile does not show a hint of a doublet. Therefore, the peak broadening is more consistent with continuous distributions of lattice spacings due to certain nonuniform distortions than with two different fixed lattice spacings expected in the case of monoclinic distortion. We would also like to note that random orientation of local JT distortions will not lead to the systematic peak broadening observed in the neutron diffraction. A more plausible explanation of this anomalous peak broadening is provided by the PDF analysis as described below.

B. Pair density function

In the following, we will discuss the neutron pair density function, which provides us with information on the local arrangement of Jahn-Teller orbitals. Plots in Fig. 5 show the neutron PDFs $G(r)$ of $LiNiO_2$ (sample 1) directly comparing the two end temperatures 10 and 585 K. One can immediately notice the two most important features in the PDF, which are not directly accessible from diffraction patterns. First, the nearest-neighbor peak in the PDF shows a double-peak structure which is a direct confirmation of elongated octahedra due to local JT distortions. Such a double peak structure has been previously observed with extended x-ray absorption fine structure (EXAFS),[14,15] but here it is seen with diffraction. However, the result rules out the possibility of the orbital frustration recently suggested by Reynaud *et al.*[13] The orbital degeneracy between equally occupied $3d_{z^2-r^2/3}$ and $3d_{x^2-y^2}$ orbitals as suggested by them would lead to equal distribution of long and short bonds, which is in a clear contradiction with our observation. Our result shows the weight is approximately 2:1 for short and long Ni—O bonds, which is consistent with the JT distortion with the $3d_{z^2-r^2/3}$-type orbital that elongates NiO_6 octahedra along the local *z* axis.

The most remarkable feature is the inversion of PDF peak heights around 80–100 Å. While the short-range peaks below 50 Å are taller at lower temperatures reflecting the effect of thermal vibration, an opposite, quite unexpected trend is seen for the long-range peaks beyond 100 Å. Figure 6 shows the temperature dependence of several PDF peak heights. It is clearly seen in Fig. 6(c) that the peaks beyond 100 Å increase in height with temperature. A possible interpretation of this unusual effect is domain formation at low temperatures, which would lead to a loss of medium-range atomic correlations. This interpretation is consistent with the broadening of the Bragg peaks shown in Fig. 3. We will discuss below what can possibly induce a temperature-dependent domain effect. Figure 6 suggests that both short-range and long-range peaks saturate beyond 400 K. We note that this temperature is close to the critical temperature found from the Rietveld refinement shown in Fig. 4.

C. Comparison with similar compounds

Conventionally PDFs are used mostly for the study of short-range atomic correlations. This, however, is in large part due to the instrumental *Q* resolution, as discussed above. The NPDF diffractometer used in this work was designed to allow high-resolution high-intensity neutron diffraction suitable for long-range PDF analysis. In order to confirm this capability we have compared the PDFs of four samples from three different compounds with similar triangular symmetry. Plots in Fig. 7 show the ratio between PDF peak heights at low temperature (G_{LT}) and at high temperature (G_{HT}) for $LiNiO_2$ (samples 1 and 2), $LiVO_2$ and $Na_{0.75}CoO_2$. The hori-

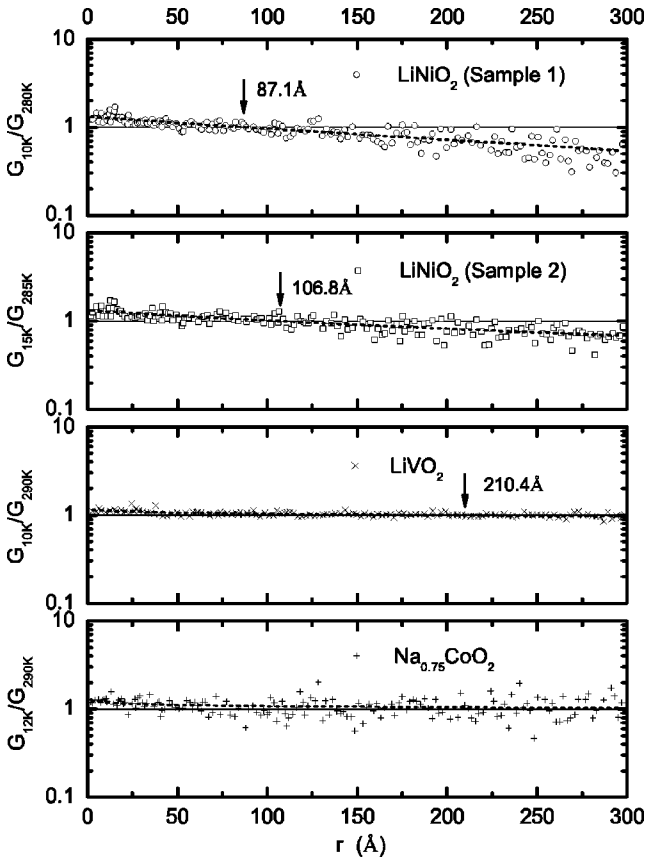

FIG. 7. The peak-height ratio for local maxima observed in the PDFs of (a) $LiNiO_2$ (sample 1), (b) $LiNiO_2$ (sample 2), (c) $LiVO_2$, and (d) $Na_{0.75}CoO_2$ compared between the lowest temperature and the room temperature. In each plot, the *x* axis represents the distances at the lower temperature. The dashed lines are fits to the logarithmic equations.

zontal axes of the plots represent the distances at low temperatures 10–15 K. The axes for the high-temperature PDFs were rescaled down for thermal expansion so that the peak positions match between the two temperatures. At short distances the ratio is larger than unity for all of the four samples, indicating that the height of the peaks at short range are sharper at low temperatures as expected. On the other hand, peak height shows quite a different behavior at longer distances. The ratio is smaller than unity for two different $LiNiO_2$ samples, while for $LiVO_2$ or $Na_{0.75}CoO_2$ it tends to unity. Note that the PDF peaks at long distances do not reflect single atomic distances, but aggregation of several overlapping peaks close enough to merge into single peaks. Therefore, their peak width is determined by the cutoff in *Q*, rather than thermal vibration. It should thus be independent of temperature, as in the case of $LiVO_2$ or $Na_{0.75}CoO_2$. This comparison confirms that the observed temperature dependence at long range for $LiNiO_2$ is not an instrumental artifact but a true, unusual feature of this compound.

If the observed unusual temperature dependence is due to domain formation, the size of the domain can be roughly estimated from the crossover point of the temperature-dependent peak height. When fitted with logarithmic functions, the lines cross unity at 87.1 and 106.8 Å for samples 1 and 2, respectively. Therefore, it is possible that the domain size is dependent upon the defect concentration in $Li_{1-x}Ni_{1+x}O_2$. However, it is interesting to note that this effect is not due to domain wall pinning by defects, since sample 2, which has a higher defect concentration, shows a larger domain size.

For $LiVO_2$, the effect was barely observable with the crossover point at 210.4 Å, so that a similar, but weaker effect may be present in this compound. It is possible that V^{3+} ($t_{2g}{}^2e_g{}^0$) also has local Jahn-Teller distortion, but the magnitude of distortion must be smaller for the t_{2g} orbital than for the e_g orbital in Ni^{+3} ($t_{2g}{}^6e_g{}^1$). On the other hand, the effect appears to be completely absent for $Na_{0.75}CoO_2$. Co^{3+} ($t_{2g}{}^6e_g{}^0$) ions in the low-spin configuration do not have Jahn-Teller distortions. While doped holes could induce local JT distortion around Co^{4+} ($t_{2g}{}^5e_g{}^0$ or $t_{2g}{}^4e_g{}^1$) the density of locally JT distorted sites in $Na_{0.75}CoO_2$ may be too low (1/4) for orbital ordering to take place.

IV. ANALYSIS OF THE RESULTS

A. Local order of Jahn-Teller orbitals

Since we now know from the PDF that the NiO_6 octahedra are locally Jahn-Teller distorted in $LiNiO_2$, it is important to ask whether they form any ordered pattern or simply distribute randomly as claimed by previous works.[14,18] We have already shown that the Rietveld refinement results are not consistent with the latter argument. A closer look at the PDF profiles gives us another clue to this question. For $LiNiO_2$ the strong PDF peak around 2.87 Å consists of the in-plane Ni—Ni, Li—Li, or O—O nearest-neighbor distances. Figure 5(b) shows that this peak has two shoulders, one at 2.69 Å and the other at 3.09 Å. They correspond to the shortest O—O distances across the Ni layer and the Li layer, respectively. These two are reasonably apart from the central peak at 2.87 Å, and are sensitive to the distortions in the oxygen plane. It is easy to imagine that in a structure with randomly oriented JT distortions such O—O distances will become widely distributed and the shoulders will be smeared. Figure 8 illustrates a possible distortion pattern when the long bonds are randomly oriented. The thick lines represent different possible, if not all, O—O distances across the Ni layer. There are at least seven different O—O distances between 2.60 and 2.85 Å according to this pattern, and the O—O peak will become broad and weak. In the low-temperature PDF profiles, however, those shoulders are clearly identifiable just as in the undistorted structure, demonstrating that random orientation of the local JT distortion is unlikely. In addition, even the Ni—O nearest-neighbor distance is subject to a wide distribution, which could blur the split of the nearest-neighbor Ni—O peak. Thus in general, the PDF peaks are expected to be wide and rather featureless if the local JT distortion is randomly oriented, while the measured PDF is rich in detailed sharp features. Thus we conclude that the random JT model does not agree with the observation.

There are many possible patterns of orbital ordering. We considered several model structures, which are summarized

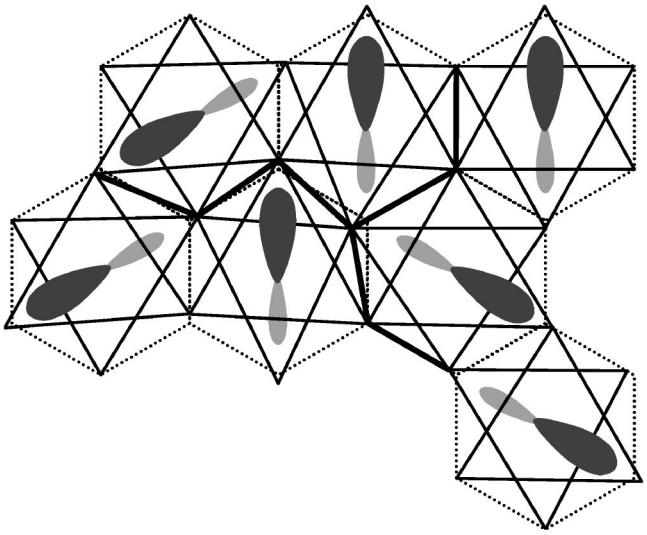

FIG. 8. A possible distortion pattern of the randomly oriented Jahn-Teller orbitals when there is no *c* axis bucking of the oxygen plane. Thick solid lines show examples of possible O—O distances across Ni layer, which range from 2.60 to 2.85 Å. The black-grey lobes denote the orientations of Ni^{3+} local $3d_{z^2-r^2/3}$ orbitals.

in Fig. 9. These model structures were refined using the PDFFIT program[25] to optimize agreement with the measured PDF. The level of agreement was evaluated by the *R* factor, which is the average of the square of the difference between the model PDF and the measured PDF. The atomic positions in the model structure were improved by the least square fit to minimize the *R* factor. The results are summarized in Fig. 10. The average $R\bar{3}m$ structure is the one with no local Jahn-Teller distortions. In all other models, the directions of the long O—Ni—O axes are depicted with double-sided lobes. Among them the collinear, or the ferro-orbital, corresponds to $NaNiO_2$ (Ref. 16) when the lattice angle parameter γ deviates from 90°. Other models involve noncollinear ordering of local JT distortions of the $3d_{z^2-r^2/3}$ orbitals, with the local *z* axis varying from site to site. While the zig-zag model breaks the threefold symmetry and will result in macroscopic distortion of the lattice, in other noncollinear models the local JT distortions point to all three possible directions with equal weight, and thus will not induce cooperative in-plane distortions.

The trimer model shown in Fig. 9, however, has an important characteristic that is not found in the monoclinic (ferro-orbital) or the zig-zag structure. Without the JT distortion three NiO_6 octahedra pointing to three different directions may be nicely put together on a plane. However, with JT distortions which elongate some of the Ni—O distances they cannot be accommodated in a flat plane (see Fig. 11). Thus the JT distortions are *frustrated* in this configuration, resulting in further distortion of the NiO_2 plane and NiO_6 octahedra with all of O—Ni—O bond angles deviating from 180°. Three long *z* axes of NiO_6 octahedra connect to, and share, an oxygen ion, but this oxygen ion is displaced along the *c* axis out of the originally flat plane. At the same time the oxygen ions on the opposite plane shift mainly parallel to the plane. Consequently the NiO_2 plane no longer

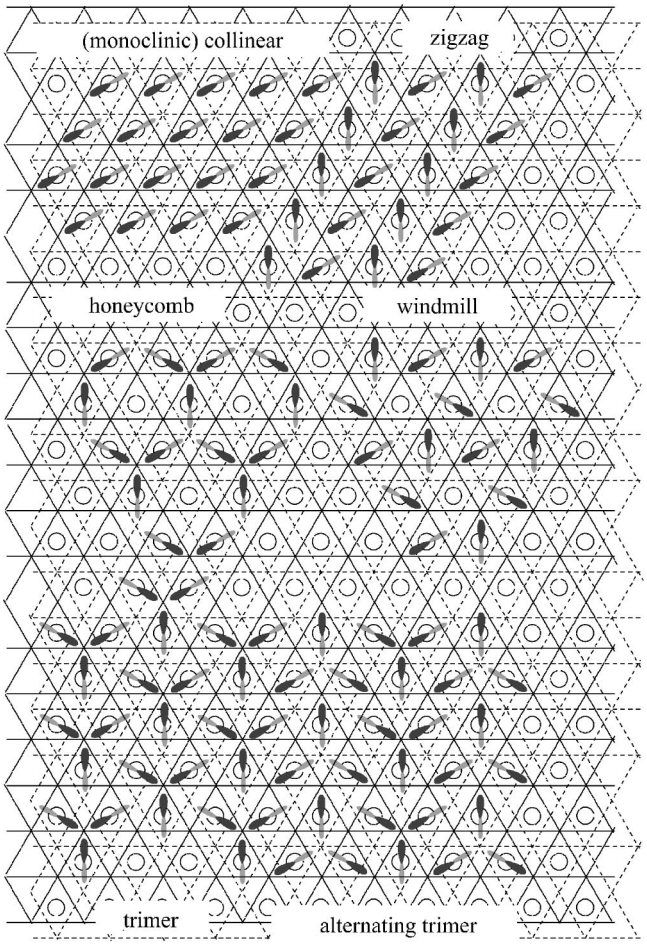

FIG. 9. An illustration of possible short-range ordering of Jahn-Teller orbitals that we have tested with PDF refinement. Open circles denote Ni sites while solid and dashed lines are upper and lower oxygen planes, respectively.

retains inversion symmetry. The Ni—O distances are split into four different bond lengths that naturally fit the shape of the nearest-neighbor peak. From the PDF refinement, the long bonds are found at 2.04 and 2.06 Å while the short bonds are at 1.90 and 1.96 Å, so the average lengths for long and short Ni—O bonds are 2.05 and 1.93 Å, respectively. The bond lengths from the $C2/m$ model were found at slightly shorter distances of 2.04 and 1.91 Å, respectively. The amount of JT distortion estimated from this study is a bit smaller than the result of an *ab initio* calculation,[26] but close to what was estimated from EXAFS measurement.[14] The fitting range as shown in Fig. 10 is up to 5.2 Å, which is slightly larger than the size of one trimer unit. We note that the intensity around 3.5 Å is smaller for all the models compared to the experimental PDF. This systematic deviation appears to be due to experimental errors, most likely related to the correction for inelastic intensities.

The results summarized in Fig. 10 show that the average $R\bar{3}m$ model fairly well reproduces the features beyond the first peak, but badly fails to describe the JT split of the first peak. While the PDF of other models we have tried obviously do not reproduce the measured PDF, apparently the agreements were the best for the monoclinic $C2/m$ and the

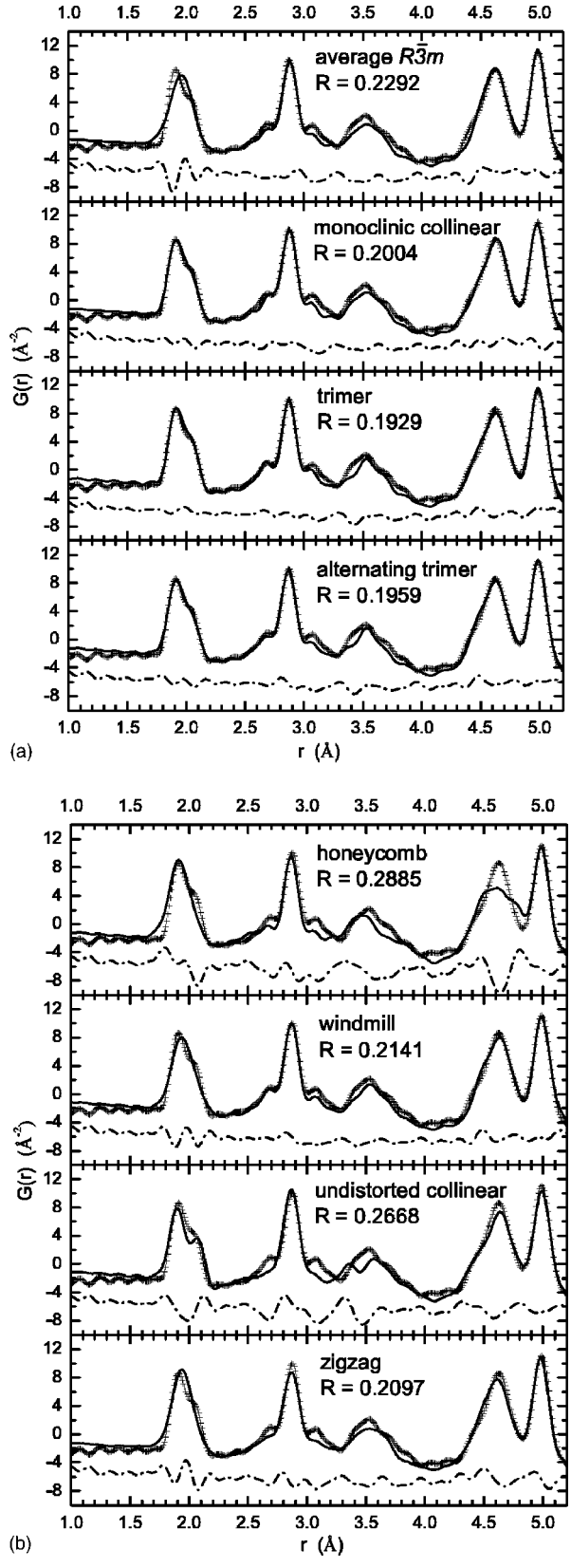

FIG. 10. Results of short-range pair density function refinements with several tried models. The crosses are the measured PDF at 10 K, and the solid and dash-dotted lines are the calculated PDF and its difference from the data, respectively. The *R* factors are shown in the plots.

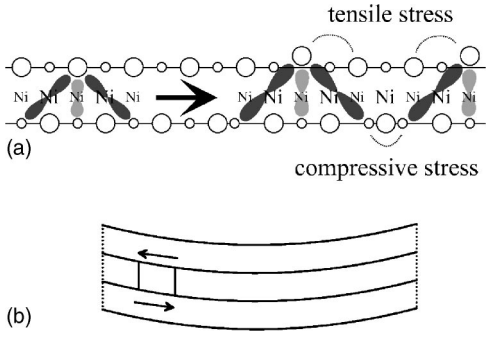

FIG. 11. (a) A lateral view of a single NiO_2 slab. Double-sided lobes are Ni $3d_{z^2-r^2/3}$ orbitals with long Ni—O bonds, and empty circles are oxygen sites. For either oxygen or nickel site, those closer or farther from the viewer are represented by relative sizes. For Ni^{3+} orbitals, black and gray lobes denote closer and farther positions, respectively. (b) A lateral view of a stack of multiple slabs. The arrows indicate the direction of monoclinic shear. The dotted line is the domain boundary, beyond which the curvature reverses.

trimer models. The asymmetric shape of the first peak is closely reproduced by both models. The trimer models show a better agreement for the O—O correlations around 3 Å, while the monoclinic model does better for the slightly longer range. In the case of the monoclinic model, however, the comparison with the Rietveld refinement suggests that it is not likely the true local structure. While the cooperative in-plane shift of the oxygen layers conveniently reproduced the JT split, this shift badly failed to realize in the Rietveld refinement. Compared to the $NaNiO_2$ structure, the collinear model shown in Fig. 10 has the oxygen ion pushing against the Li site, under which situation the negative monoclinic shear is unlikely (see Fig. 4). The unlikeliness of such uniform shift is also reflected in a relatively poor agreement of the O—O correlation peaks between 2.6 and 3.2 Å. Therefore, the monoclinic collinear structure obtained by the PDF refinement is supposed to be an accidental one. We also stress that the ferro-orbital arrangement is inconsistent with observed magnetic properties of $LiNiO_2$, which is in clear contrast with that of $NaNiO_2$.

All these points and a relatively large *R* factor make the monoclinic structure less favorable than the trimer models. Thus, it is most likely that the trimer models are the actual short-to-medium range structure. Unfortunately, the reciprocal space Rietveld refinement with the trimer models are not possible, since the superlattice peaks due to the orbital ordering are mostly very weak in intensity. We need a single crystal diffraction study to detect these superlattice peaks. In the following, we will present more arguments why the trimer structures are most likely the true local structure, and among them, the fully ordered trimer structure must be the ground state structure.

B. Origin of the limited correlation length

We have mentioned above that the JT distortion is locally frustrated in the trimer ordering model, which results in the distortion of the NiO_6 octahedra. We now discuss the impli-

cation of this local distortion to the long-range order. The trimer ordering of JT distortion induces displacement of the oxygen ion shared by three JT distorted octahedra out of the plane, and stresses between oxygen ions. At the same time, the three other long Ni—O bonds pointing towards the opposite plane push the oxygen ions sideways, creating a compressive stress against surrounding oxygen ions [see Fig. 11(a)]. As a result, the NiO_2 slab becomes slightly curved. Since the curved slab is inconsistent with the average structure, this results in yet another level of frustration, and prevents the trimer ordering from becoming the long-range order. Therefore it is reasonable to assume that domains will be formed consequently to accommodate the curvature. The curving of the layer will be correlated along the *c* axis [Fig. 11(b)], producing three-dimensional domains. In a perfect structure domains will be regular and periodic, but any defects could pin them, and make them random. Thus the structural coherence is likely to be limited by the domain size. This explains quite well the observed crossover behavior of the PDF shown in Fig. 7 and the Bragg peak broadening shown in Fig. 3(b). As shown in Fig. 7 two samples with different defect densities have different crossover points, suggesting different domain sizes. This supports our view that the domains are pinned by defects. However, as mentioned earlier the fact that sample 1 has a smaller domain suggests that pinning does not occur at the domain walls. It is more likely that defects allow larger deformation and a larger domain size. On the other hand, the alternating trimer model corresponds to the trimer model with a narrow one-dimensional domain with alternating curvature. This model does not lead to the nanoscale frustration, and does not explain the domain formation and the crossover phenomenon in Fig. 7.

It should be pointed out that the Bragg peak broadening shown in Fig. 3 should not be directly interpreted in terms of the structural coherence length. It more strongly reflects the distribution of lattice spacings induced by the monocliniclike distortion. Since the shear stress tensor has a center of symmetry at the center of the domain, the domain cannot have a monoclinic symmetry as a whole. This also explains why we do not observe a monoclinic peak splitting, which otherwise is expected as shown in the inset of Fig. 3(a). We emphasize that such a bent slab will not disturb the lattice spacings of (0 0 *l*) or (*h k* 0) planes very much. On the other hand, for the planes nearly perpendicular to the orientation of $3d_{z^2-r^2/3}$ Jahn-Teller orbitals, the monoclinic shear will certainly have larger effects. Indeed the peak width is strongly correlated with the angle away from the NiO_4 square basal plane of the JT distorted NiO_6 octahedron, as shown in Fig. 3(c). Therefore, we can conclude that the average structure of $LiNiO_2$ is still hexagonal even at low temperatures, and the monoclinicity suggested in the diffraction profiles is simply a reflection of the local stress effect.

We note that the changes in the powder diffraction peak widths [Fig. 3(b)], in the PDF peak heights [see Fig. 6(c)] and the monoclinic distortion all take place at $T_d = 375$ K. Therefore, it is likely that this temperature is where the trimer ordering begins and distorts the local as well as global lattice structure. We note again that this temperature is very close to the temperature where the dc susceptibility anomaly was observed and interpreted in terms of the orbital exchange interaction.[13]

C. Discussions on possible implication to magnetism

To understand the magnetic properties of $LiNiO_2$ it is important to make measurements on samples with the least amounts of defects, on which their properties are strongly dependent.[7,9,24] The most prevalent type of defect is believed to be Ni substitution of Li ions. Such substitution can introduce interplanar ferromagnetic coupling between Ni layers. This interplanar exchange is supposed to be stronger than the intraplanar one since the Ni—O—Ni bond angle for an interplanar Ni pair through substitutional Ni is nearly 180°, while that of an intraplanar one is close to 90°. With low Ni impurity concentrations $x \leqslant 0.02$, however, the ferromagnetic coupling is weak and the material shows a tendency for antiferromagnetic fluctuations.[24] For the near-stroichiometric composition, the intraplanar exchange must be the primary component of the magnetic coupling, and the orbital ordering is expected to play an important role. While magnetic measurements may be masked by small amounts of impurity, the orbital-lattice interaction should certainly be observable. The comparison between the two samples in our study suggests not only that the proposed orbital ordering is very likely to be intrinsic, but also that it persist up to moderate impurity concentrations.

What is particularly interesting is the obvious difference between $NaNiO_2$ and $LiNiO_2$. In the case of $NaNiO_2$, $3d_{z^2-r^2/3}$ orbital orientation is collinear and the intraplanar exchange is ferromagnetic, while the interplanar exchange is antiferromagnetic.[17] According to the Kanamori-Goodenough rule the 90° exchange can lead to ferro-orbital ordering via the spin-orbit decoupling when the Hund coupling between oxygen holes is negligible. On the other hand, the situation of $LiNiO_2$ is distinctly unclear. Experimentally a tendency for antiferromagnetic orbital fluctuations is observed,[4–7] which would imply triangular symmetry between neighboring orbitals is favored. However, no apparent long-range ordering has been found in $LiNiO_2$. It has been speculated that the quantum spin-orbital liquid state may be formed via orbital degeneracy,[27] but our result clearly shows that the orbital order is not in a liquid state. Mostovoy *et al.*[28] attributed the absence of orbital ordering in $LiNiO_2$ to an impurity effect, while our analysis argues against it. Although the effect of impurity is apparent in $LiNiO_2$, our results do not point to ferro-orbital ordering as an intrinsic limit, but suggest a completely different kind of orbital ordering, involving trimer local ordering of orbitals.

Interestingly, the trimer model provides a possible interpretation for the coexistence of ferromagnetic and antiferromagnetic spin fluctuations without considering an impurity effect. The three $3d_{z^2-r^2/3}$ orbitals forming a trimer could form a spin-singlet state if the nearest-neighbor exchange among them is negative. While the Goodenough-Kanamori-Anderson rules suggest a positive exchange, the trigonal crystal-field effect at the oxygen site could result in an antiferromagnetic exchange, as pointed out recently.[29] On the two-dimensional plain, there are two choices how the trimer

units can be arranged as shown on the bottom part of Fig. 9. In the basic trimer model, the units again retain triangular symmetry, subject to geometrical fluctuations at the trimer cluster level. On the other hand, the alternating trimer model loses the triangular symmetry, so that we cannot rule out the possibility of short-range magnetic ordering that lifts geometrical frustration within the trimer. It is most likely that the triangular arrangement of trimers prevails in the bulk of the system (domain with curved plane), and the alternating pattern is found at the boundary between the domains. A recent suggestion on the presence of ferromagnetic clusters within the plane[30] could be attributed to such a domain boundary effect. We suspect that this domain boundary can restrict the extent of antiferromagnetic fluctuations, effectively reducing possible consequences of quantum fluctuations. The curved lattice in the trimer model implies another interesting complication in achieving a stable ground state. Since one domain with a positive curvature has to be contiguous to another domain with a negative curvature, the triangular symmetry again leads to a morphological frustration between three neighboring domains similarly to magnetic frustration. In the presence of impurities, which may pin the domain walls, the configuration of the frustrated domains will be irregular. We suspect that $LiNiO_2$ is a system where its macroscopic physical properties are determined by several layers of coexisting atomic–short-range–intermediate-range frustrations. The frustrated domains may lead to interesting elastic properties, which should be detectable by a careful measurement on the elastic tensor of a single crystal.

V. CONCLUSIONS

We have performed a temperature-dependent neutron diffraction study of $LiNiO_2$ in order to probe the local ordering of Ni^{3+} Jahn-Teller orbitals. From the combined analysis of the real space pair distribution function and the reciprocal space diffraction profile, we conclude that the JT distortions in this material are not randomly oriented, but form local ordering. The ordering is quite different from the collinear type found in $NaNiO_2$, and is most likely the trimer type, where three $3d_{z^2-r^2/3}$ orbitals point towards the shared oxygen site. In this model, the shared oxygen site will be displaced away from the NiO_2 plane, forcing the NiO_2 plane to have a curvature. Since the neighboring planes will have a similar curvature and the curvature prevents the trimer ordering from becoming long-range order, the system is composed of nanoscale domains of local trimer order. A signature of such a curved plate can be found in the diffraction profile as the monoclinic like peak broadening. The temperature for the short-range trimer ordering to take place is estimated to be $\sim$375 K. The unconventional magnetism observed in this material may be explained in the context of the interplay between Ni^{3+} $3d_{z^2-r^2/3}$ orbitals, trimer units, and domains under a triangular symmetry.

ACKNOWLEDGMENTS

The authors thank D. Khomskii, A. R. Bishop, A. Saxena, A. Stepanov, and R. Hayn for useful discussions. This work was supported by the National Science Foundation through Grant No. DMR01-02565 and by the Laboratory Directed Research and Development Program of Oak Ridge National Laboratory, managed by UT-Battelle, LLC, for the U.S. Department of Energy under Contract No. DE-AC05-00OR22725. This work has benefited from the use of NPDF at the Lujan Center at Los Alamos Neutron Science Center, funded by DOE Office of Basic Energy Sciences and Los Alamos National Laboratory funded by Department of Energy under Contract No. W-7405-ENG-36. The upgrade of NPDF has been funded by NSF through Grant No. DMR 00-76488.

*Present address: NIST Center for Neutron Research, National Institute of Standard and Technology, Gaithersburg, MD 20899, USA and University of Maryland, College Park, Maryland 20742, USA.

[1] K. Hirakawa, R. Osborn, A. D. Taylor, and K. Takeda, J. Phys. Soc. Jpn. **59**, 3081 (1990).
[2] P. W. Anderson, Mater. Res. Bull. **8**, 153 (1973).
[3] J. P. Kemp, P. A. Cox, and J. W. Hodby, J. Phys.: Condens. Matter **2**, 6699 (1990).
[4] H. Yoshizawa, H. Mori, K. Hirota, and M. Ishikawa, J. Phys. Soc. Jpn. **59**, 2631 (1990).
[5] K. Hirota, Y. Nakazawa, and M. Ishikawa, J. Phys.: Condens. Matter **3**, 4721 (1991).
[6] A. Rougier, C. Delmas, and G. Chouteau, J. Phys. Chem. Solids **57**, 1101 (1996).
[7] A.-L. Barra, G. Chouteau, A. Stephanov, and C. Delmas, J. Magn. Magn. Mater. **177–181**, 783 (1998).
[8] J. N. Reimers, J. R. Dahn, J. E. Greendan, C. V. Stager, G. Liu, I. Davidson, and U. von Sacken, J. Solid State Chem. **102**, 542 (1993).
[9] K. Yamaura, M. Takano, A. Hirano, and R. Kanno, J. Solid State Chem. **127**, 109 (1996).
[10] M. Corti, S. Marini, A. Rigamonti, V. Massarotti, and D. Capsoni, J. Appl. Phys. **79**, 6621 (1996).
[11] A. Bajpai and A. Banerjee, Phys. Rev. B **55**, 12 439 (1997).
[12] Y. Kitaoka, T. Kobayashi, A. Koda, H. Wakabayashi, Y. Nino, H. Yamakage, S. Taguchi, K. Amaya, K. Yamaura, M. Takano, A. Hirano, and R. Kanno, J. Phys. Soc. Jpn. **67**, 3703 (1998).
[13] F. Reynaud, D. Mertz, F. Celestini, J.-M. Debierre, A. M. Ghorayeb, P. Simon, A. Stepanov, J. Voiron, and C. Delmas, Phys. Rev. Lett. **86**, 3638 (2001).
[14] A. Rougier, C. Delmas, and A. V. Chadwick, Solid State Commun. **94**, 123 (1995).
[15] I. Nakai, K. Takahashi, Y. Shiraishi, T. Nakagome, and F. Nishikawa, J. Solid State Chem. **140**, 145 (1998).
[16] L. D. Dyer, B. S. Borie, Jr., and G. P. Smith, J. Am. Chem. Soc. **76**, 1499 (1954).
[17] P. F. Bongers and U. Enz, Solid State Commun. **4**, 153 (1966).

[18] C. Pouillerie, E. Suard, and C. Delmas, J. Solid State Chem. **158**, 187 (2001).
[19] V. Bianchi, D. Caurant, N. Baffier, C. Belhomme, E. Chappel, G. Chouteau, S. Bach, J. P. Pereira-Ramos, A. Sulpice, and P. Wilmann, Solid State Ionics **140**, 1 (2001).
[20] Th. Proffen, T. Egami, S. J. L. Billinge, A. K. Cheetham, D. Louca, and J. B. Parise, Appl. Phys. A: Mater. Sci. Process. **74**, S163 (2002).
[21] A. Larson and R. B. von Dreele, *GSAS: General Structure Analysis System*, Los Alamos National Laboratory, 1994.
[22] T. Egami and S. J. L. Billinge, *Underneath the Bragg Peaks: Structural Analysis of Complex Materials* (Pergamon, Amsterdam, 2003).
[23] P. F. Peterson, M. Gutmann, Th. Proffen, and S. J. L. Billinge, J. Appl. Crystallogr. **33**, 1192 (2000).
[24] F. Reynaud, A. M. Ghorayeb, Y. Ksari, N. Menguy, A. Stephanov, and C. Delmas, Eur. Phys. J.: Appl. Phys. **14**, 83 (2000).
[25] Th. Proffen and S. J. L. Billinge, J. Appl. Crystallogr. **32**, 572 (1999).
[26] C. A. Marianetti, D. Morgan, and G. Ceder, Phys. Rev. B **63**, 224304 (2001).
[27] L. F. Feiner, A. M. Oles, and J. Zaanen, Phys. Rev. Lett. **78**, 2799 (1997).
[28] M. V. Mostovoy and D. I. Khomskii, Phys. Rev. Lett. **89**, 227203 (2002).
[29] A.-M. Dar, R. Hayn, and J.-L. Richard, Europhys. Lett. **61**, 803 (2003).
[30] J. van Duijn, B. Gaulin, S. Park, S.-H. Lee, and J. Copley, Bull. Am. Phys. Soc. **48**, N31.006 (2003).